α-Tricalcium phosphate hydrolysis to hydroxyapatite at and near physiological temperature

C. DURUCAN, P. W. BROWN
Materials Research Laboratory, The Pennsylvania State University, University Park, PA 16802, USA
E-mail: ext@psu.edu

The kinetics of hydroxyapatite (HAp) formation by direct hydrolysis of α-tricalcium phosphate (α-TCP) [α-$Ca_3(PO_4)_2$] have been investigated. Transformation kinetics were examined for reactions at 37 °C, 45 °C and 56 °C by isothermal calorimetric analysis. Setting times and morphologies of the resultant HAp were found to be strongly dependent on reaction temperature. XRD analysis accompanied by FTIR confirmed that phase pure calcium-deficient hydroxyapatite (CDHAp) [$Ca_{10-x}(HPO_4)_x(PO_4)_{6-x}(OH)_{2-x}$] was formed. Complete reaction occurs within 18, 11, 6.5 h at 37, 45 and 56 °C, respectively. The extent of HAp formation differs for particulate slurries and pre-shaped forms of reactant α-TCP. Formation of hydroxyapatite in pre-formed pellets was hindered due to limited water penetration, but enhanced with the presence of NaCl as a pore generator. Regardless of the precursor characteristics and temperature, HAp formation is characterized by an initial period of wetting of the α-TCP precursor, an induction period and a growth period during which the bulk transformation to HAp occurs. The microstructures of the resultant HAp at all temperatures were generally similar and are characterized by the formation porous flake-like morphology. Microstructural coarsening was observed for the CDHAp formed above the physiological temperature. The hardening generated by the hydrolysis reaction was demonstrated using diametrical compression tests. The original tensile strength of 56% dense α-TCP increased from 0.70 ± 0.1 MPa to 9.36 ± 0.4 MPa after hydrolysis to CDHAp at 37 °C, corresponding to a density of 70%.

1. Introduction

Hydroxyapatite (HAp) has been used for hard tissue replacement and augmentation due to its biocompatibility and osteoconductive potential. Because of the compositional similarity to hard tissues, such implants may be superior to alternative materials. Associated with its biocompatibility, there is interest in HAp for applications involving orthopaedics [1, 2] and dentistry [3, 4]. Alternatively, HAp may be coated onto metal prostheses as a means to promote bone intergrowth, thereby improving the bond between native tissue and prosthesis [5]. In addition there is interest in HAp-based composites, which combine the osteoconductive potential of HAp with the biodegradable nature of some organic materials [6–8].

Reactions by which HAp can be formed at low temperatures by a cement-type reaction involving dissolution and precipitation have been identified [9]. These typically involve acid-base reaction between particulate calcium phosphate precursors or direct hydrolysis of a particulate solid calcium lacking a true solubility. For the latter instance Monma and Kanazawa first reported that α-tricalcium phosphate (α-TCP) sets in the presence of water to form phase-pure HAp [10].

The HAp produced by a cement-type reaction may exist over a compositional range and can be characterized in terms of its Ca/P ratio. Stoichiometric HAp, $Ca_{10}(PO_4)_6(OH)_2$ has a Ca/P ratio of 1.67, while CDHAp, $Ca_{10-x}(HPO_4)_x(PO_4)_{6-x}(OH)_{2-x}$ may have Ca/P ratios extending to 1.5. For fully calcium-deficient HAp, x is equal to unity. Hydrolysis of α-TCP to HAp at low temperature is particularly attractive for several reasons. It utilizes a single precursor and forms fully calcium-deficient HAp, which is more soluble than stoichiometric HAp and therefore may be incorporated into bone more readily by osteocytes. The suitability for use *in vivo* is based on findings that reaction kinetics can be improved by chemical treatment of the reactant powder or by certain additives [11]. Fast setting times are important for the powders used as moldable cements for repair of bone defects. Such an implant can be also shaped prior to hardening and placed into the defect site. This facilitates intergrowth and depending on micro-

structure, resorption of implanted material may be possible.

Previous research showed that α-TCP slurries can rapidly hydrolyze to HAp [12, 13]. However, to achieve clinical relevance it must be established that low water-to-solid ratio α-TCP compacts can also react to form HAp. This present work compares hydrolysis kinetics for HAp formation at and near physiological temperatures for particulate slurries and pre-formed pellets of α-TCP. The microstructural development of HAp monoliths and the effect of an artificial pore generator, NaCl, on the hydrolysis rates are described. The tensile strength of the hydrolysis product HAp was also examined in comparison with the original strength values for nonhydrated α-TCP. Finally, the relationship between the extent of HAp formation and mechanical property development was established.

2. Materials and methods

2.1. Precursor processing and HAp formation

The formation of CDHAp was accomplished by the following hydrolysis reaction:

$$3Ca_3(PO_4)_2 + H_2O \rightarrow Ca_9(HPO_4)(PO_4)_5OH$$

α-TCP was prepared by a solid state reaction between reagent grade calcium carbonate ($CaCO_3$) and thermally synthesized calcium pyrophosphate ($Ca_2P_2O_7$) at 1150 °C for 1 h. The goal of solid state reaction was to make powder with high reactivity. $CaCO_3$ and $Ca_2P_2O_7$ were mixed in equimolar proportions required to produce TCP and Sweco milled for 24 h before firing. After firing, the TCP was air quenched to avoid formation of the lower temperature β-polymorph of TCP. Fired α-TCP was ground by using mortar and pestle and milled to an average particle size of 3.3 μm in equivalent spherical diameter. Stoichiometric HAp was formed by an acid-base reaction between particulate dicalcium phosphate dihydrate ($CaHPO_4 \cdot 2H_2O$) and tetracalcium phosphate ($Ca_4(PO_4)_2O$) in water at room temperature, followed by air sintering at 1200 °C for 2 h [14]. Phase purity of the synthesized powders was confirmed by X-ray diffraction (XRD).

2.2. Characterization

XRD analysis was performed using a Scintag automated diffractometer. All XRD scans were performed at 0.02 °C step size and at a scan rate of 4° 2θ/min. All samples were scanned over a 2θ range of 20°–40°. Microstructural development was observed by a conventional dual stage scanning electron microscope (SEM). A Bruker Optics IFS 113 v. model spectrometer was used for fourier transform infra-red (FTIR) analysis of the hydrolysis product. IR spectra were collected using a resolution of 4 cm^{-1} and 50 scans over a range of 400 to 4000 cm^{-1}. The background data were collected for KBr substrate and subtracted out of each spectrum in order to obtain cleaner data.

2.3. Reaction kinetics

The formation kinetics of HAp from α-TCP were monitored by isothermal calorimetry. The details of the isothermal calorimetry can be found elsewhere [15, 16]. Calorimetric experiments were performed using particulate slurries and pellets of α-TCP pressed at 5.5 MPa. Isothermal calorimetry technique is based on the determination of the rate of heat evolution and total heat during α-TCP hydrolysis. All calorimetric analyses were performed at constant temperature maintained by a water bath connected to the calorimetric reaction chamber. Reaction kinetics were studied at 37, 45 and 56 °C. Solid reactants of pressed pellets or powder samples were weighed in a gold-coated copper calorimeter cup and sealed with parafilm to minimize the endothermic effects of water evaporation which contributes to the actual heat evolved. Typically 3 ml of deionized water was reacted with an equivalent mass of α-TCP. The disc-shaped pressed samples were 5.00-5.50 mm thick and 12.80 mm in diameter. The sealed calorimeter cup containing the sample and syringe containing the reactant deionized water was placed into the body of the calorimeter. The thermal equilibrium was monitored by the change in the background thermopile voltage prior to reaction. After a steady state was observed in the voltage change the reaction was started by injecting the deionized water into the calorimetry cup that initiates heat evolution. The rates of heat evolution (dQ/dt) due to the mixing of the reactants and the subsequent reactions to form HAp were measured and recorded. Total heat evolution was determined by integrating the rate data, and plots of heat evolved are presented in kJ/mol of HAp formed.

2.4. Mechanical testing

The samples for mechanical measurement were made by pressing the α-TCP precursor in a cylindrical die at a pressure of 5.5 MPa. 1.5 g of α-TCP powder were pressed. Typically, circular disc-shaped samples were 1.90–2.00 mm thick with diameters of 12.80 mm. The pressed samples were placed in storage vials filled with an equivalent mass of deionized water and the vials were floated in a closed double-wall beaker, connected to a water bath. The temperature was kept constant during HAp formation. The samples for mechanical testing were hydrated at 37 °C and 56 °C. The fracture strength values were determined using a diametrical compression test (Brazilian Test), where circular discs were compressed between two flat plates. To reduce the high compressive stresses at the loading lines a paper towel pad was inserted between the loading plates and specimens. Padding material also compensates for any surface irregularities of the specimen in contact with the Instron's flat platens and leads to a uniform load distribution. Testing was performed with a cross head speed of 0.05 cm/minute.

2.5. Density measurements

The density of the HAp monoliths formed by hydrolysis of α-TCP pellets and the densities of the pressed pellets

before hydrolysis were determined by porosity measurements. This was performed by relating the bulk density obtained using Archimede's method to the theoretical density of $2.79\,g \cdot cm^{-3}$ [17] and $2.863\,g \cdot cm^{-3}$ [18] for Ca-deficient HAp and α-TCP, respectively.

3. Results and discussion

3.1. Reaction kinetics

The rates of heat evolution (dQ/dt) during hydrolysis of particulate slurries and pressed pellets of α-TCP are illustrated in Fig. 1. The isothermal calorimetry analyzes were performed for both types of samples at 37 °C, 45 °C and 56 °C. The curves in Fig. 1 plot heat evolution in watts per mole of HAp formed against reaction times. The general appearance is the same for both types of samples. The rate of heat evolution curves show the same typical features for HAp formation from calcium phosphate precursors [16, 19, 20]. Each curve shows three heat peaks. The first peak corresponds to a maximum in rate occurring a few minutes after mixing. This very short duration step is primarily associated with wetting, initial dissolution of α-TCP and establishment of critical degrees of supersaturation. Following the initial peak is an induction peak separating mixing peak and main reaction peak. This second peak has been determined to be associated primarily with the formation of HAp [14, 21]. However, some HAp growth is also associated with the nucleation peak. The duration of this peak and the time of its occurrence are both shortened at higher hydrolysis temperatures. As the nucleation proceeds, the rate of heat evolution decreases continuously. The third peaks in the calorimetric curves are due to HAp growth. Since hydrolysis of α-TCP is strongly thermally activated, similar to nucleation peaks, the times and duration of growth peaks decrease at higher temperatures.

Fig. 2 shows the heats of reaction in kJ/mol of HAp formed. These data were obtained by integrating the rate curves with respect to time. A typical heat curve reaches a plateau at complete reaction after which no further heat is produced. Completion in this context is complete consumption of the reactants leading to the formation of HAp. An enthalpy of reaction of 133 kJ/mol is indicative of complete reaction [22]. The total amount of heat evolved during the transformation in kJ/mol of HAp differs for powder and pressed samples. The extent of heat evolution when α-TCP was hydrolyzed in pellet form was lower than when hydrolysis was carried out in powder form. This was the case for all temperatures. The total heat liberated is around 130 kJ/mol for slurry-based samples indicating that hydrolysis reached completion at each temperature. The time for complete reaction decreased to about 6.5 h from 18 h as the hydrolysis temperature was increased from 37 °C to 56 °C.

The reaction did not proceed to completion for pressed

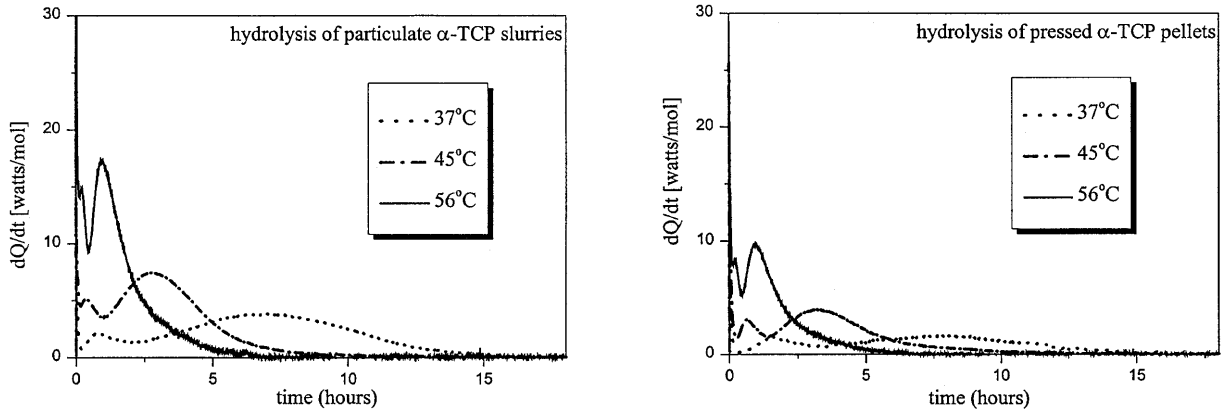

(a) (b)

Figure 1 Rates of heat evolution during HAp formation from (a) particulate slurries and (b) pressed pellets of α–TCP at 37 °C, 45 °C and 56 °C.

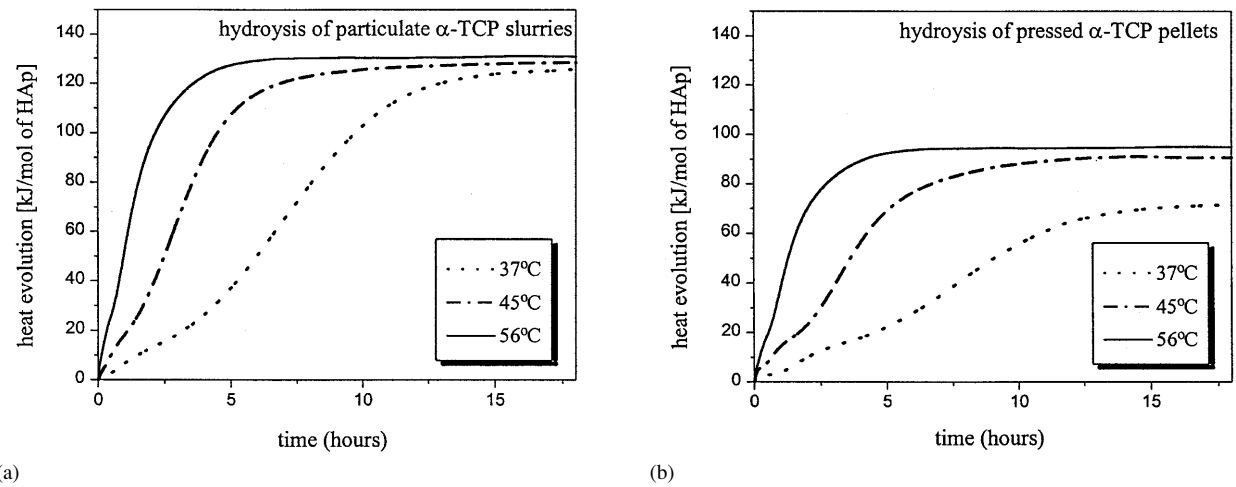

(a) (b)

Figure 2 Total amounts of heat evolved during HAp formation from (a) particulate slurries and (b) pressed pellets of α-TCP at 37 °C, 45 °C and 56 °C.

TABLE I Times for nucleation and complete reaction during HAp formation from particulate α-TCP

Hydrolysis temperature (°C)	Nucleation period (h)	Time for completion (h)
37	2.2	18
45	1	11
56	0.5	6.5

samples at the highest temperature studied (56 °C) even after 20 h. The total heat output for pressed samples was in the range of 70–95 kJ/mol after 20 h of reaction. Table I summarizes the nucleation and growth periods during hydrolysis of particulate α-TCP slurries at the studied temperatures. The changes in the slopes of heat curves correlate with the nucleation and growth peaks as illustrated in the rate curves. Induction periods of about 1.5 and 0.5 h, respectively, during which only a few kJ evolved, can be observed for the reactions at 37 °C and 45 °C for pellets. However, for the particulate α-TCP slurries, the induction period is distinguishable only for the reaction at 37 °C. This period is absent for both cases when reaction occurs at 56 °C, indicative of increasing overlap of nucleation and growth events at higher temperatures.

Extent of HAp formation at different reaction temperatures was also confirmed with companion XRD analyses. Fig. 3 shows the patterns for α-TCP and HAp formed by hydrolysis of α-TCP powder and pressed samples at 37, 45 and 56 °C. All the reactions involving slurries produced phase-pure HAp in that no residual α-TCP or any other phase could be detected. Comparison of these patterns with those for HAp formed from pressed samples indicates the presence of unreacted α-TCP even at the highest hydrolysis temperature of 56 °C.

3.2. Characterization of hydrated product

Fig. 4 shows SEM micrographs of α-TCP and typical HAp powders. The hollowed out appearance of the small granules is due to solid state reaction of the milled reactants. Consistent with the results reported by Leamy *et al*. [13] the HAp formed at the studied temperatures appears in flake-like morphology. The HAp formed at 37 °C appears in flaky- to needle-like form with smaller crystallite size. This is a result of microstructural coarsening above physiological temperature.

The comparison of FTIR spectra of the stoichiometric HAp and the product formed by hydrolysis of particulate α-TCP slurries at 56 °C for 24 h is shown in Fig. 5. The differences in FTIR spectra are indicated with arrows. The absorption bands at 630 and 3573 cm^{-1} suggest the presence of structural OH^- groups in the hydrated products. These bands are assigned to the OH^- librational mode and to the stretching mode respectively [23, 24]. The OH^- stretching band, which appears as a symmetrical and narrow peak, falls into the range of weakly hydrogen-bonded groups for absorbed H_2O. A more distinguishable OH^- band is the librational mode neighboring the principal PO_4^{3-} absorption bands at 630 cm^{-1}. The shape of this band differs for the two apatite structures, though the position remains the same. This band appears as a shoulder in HAp formed by α-TCP hydrolysis, but as a small sharp peak in the stoichiometric HAp, indicative of the structural difference. The decrease in the absorption intensity of the OH^- band suggests the formation of CDHAp, in that only one OH^- is present in the unit cell. In addition, the spectra for the hydrolysis product posses the absorption band arising from HPO_4^{2-}. A flat weak band relative to stoichiometric HAp at 872 cm^{-1} assigned as P–OH stretch of HPO_4^{2-} group, which is unique to calcium-deficient minerals [25, 26]. Thus, these data show the HAp formed to be calcium-deficient.

3.3. Effect of NaCl

It was found that particulate NaCl accelerated the initial hydrolysis rates for the pressed samples. 10 wt % and 25 wt % of NaCl particles below 70 μm in size were mixed with α-TCP and pressed at 5.5 MPa prior the hydrolysis. Fig. 6 shows the differential curves (dQ/dt vs time) for both unmodified α-TCP and NaCl-modified samples, during the first 24 h of hydrolysis at 45 °C. The data show that NaCl addition primarily modifies the nucleation of HAp in the early stages of hydrolysis. Examination of the curves indicates both the durations and the times of occurrence of the nucleation peaks are

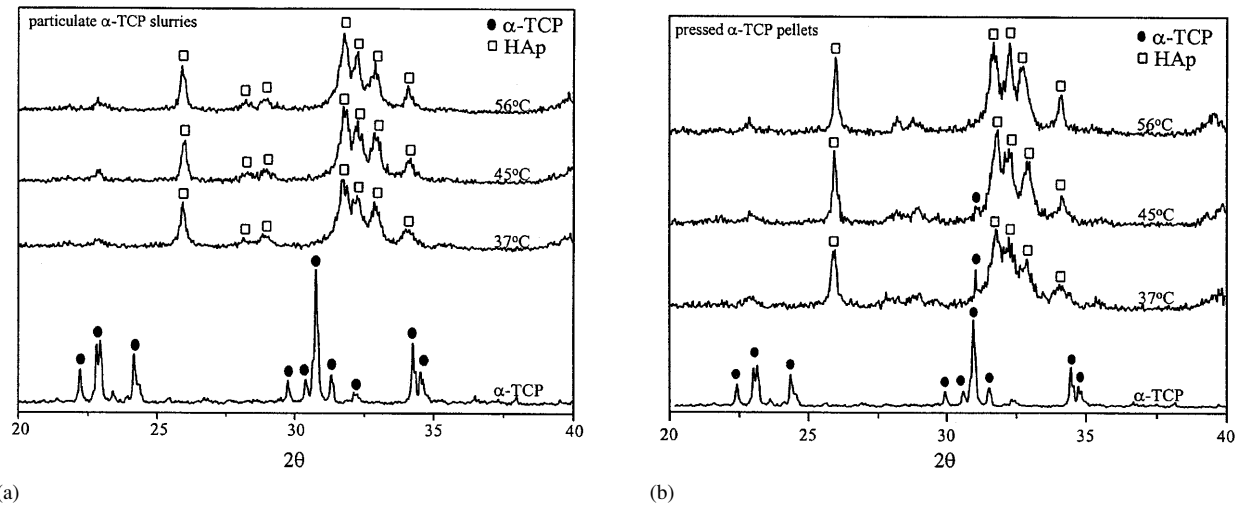

(a) (b)

Figure 3 XRD patterns of HAp formed by the hydrolysis of (a) particulate slurries and (b) pressed pellets of α-TCP.

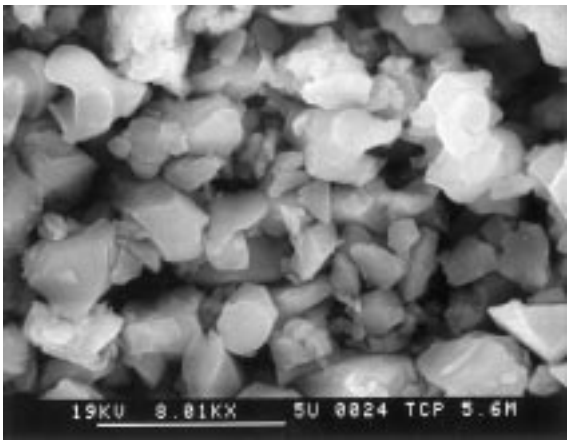

(a)

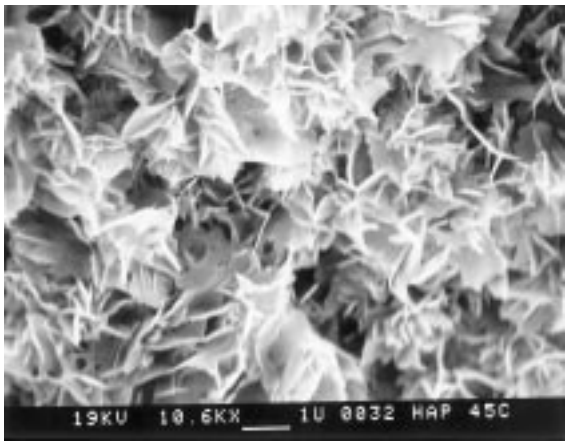

(d)

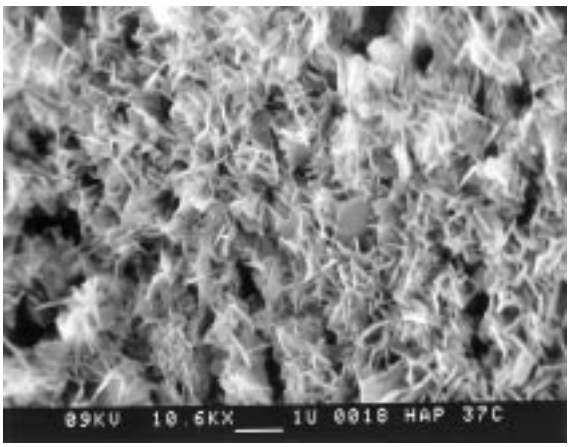

(b)

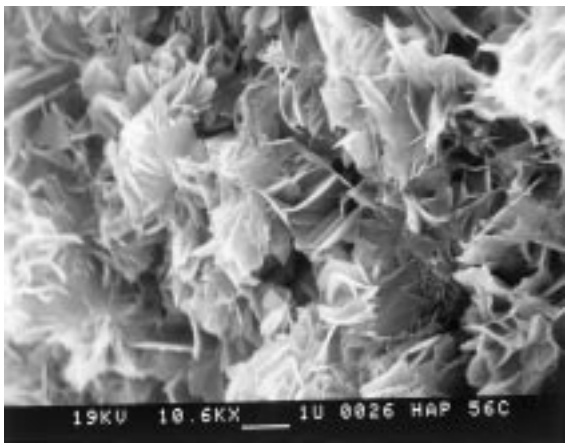

(c)

Figure 4 SEM micrograph of (a) α-TCP particles and HAp formed by hydrolysis of α-TCP particulate slurries at (b) 37 °C (c) 45 °C, and (d) 56 °C. Bar in (a) equals 5 μM; (b–d) equals 1 μM.

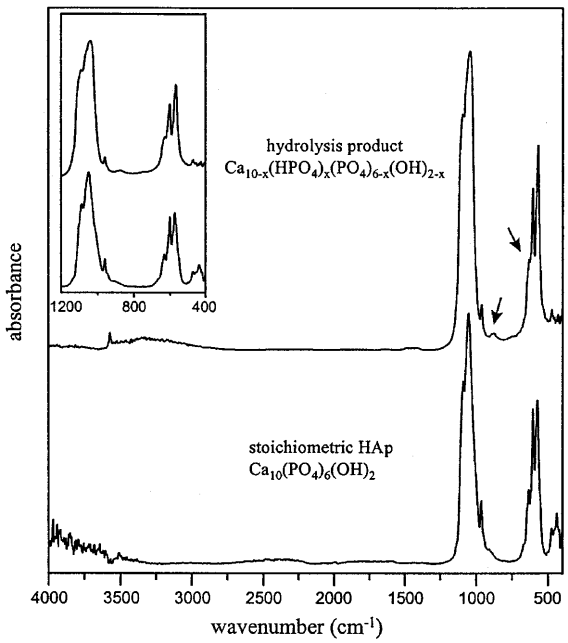

Figure 5 Comparison of the FTIR spectra of stoichiometric HAp and Ca-deficient HAp formed by hydrolysis of α-TCP at 56 °C for 24 h.

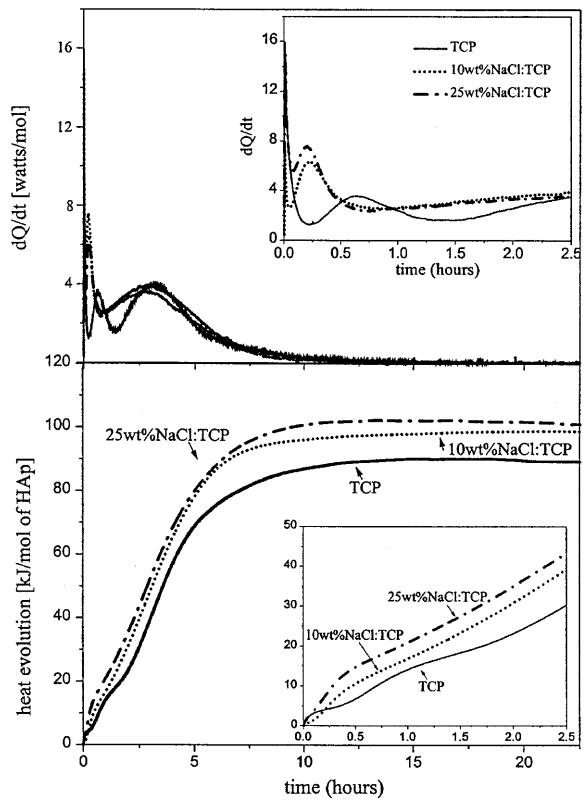

Figure 6 Rates of heat evolution and total heats evolved during hydrolysis of α-TCP compacts and NaCl modified α-TCP compacts at 45 °C.

reduced by NaCl addition. The amount of the heat evolved during nucleation also appears to increase slightly with increasing proportion of NaCl. However, the total heat evolved for each of the samples, as shown in Fig. 6, becomes approximately the same after 24 h.

A porous microstructure produced after leaching of NaCl particles during hydrolysis allowed water to penetrate and spread within the matrix more effectively. This also enhanced hydrolysis, by increasing the pathways through which water can migrate and by increasing the accessiblity of the α-TCP particles to water. Previous studies have established that a pore size between 40–100 μm is the minimum interconnection pore size showing the potential for mineralized bone ingrowth [27]. Thus, it is hypothesized that the intentionally constructed pores would serve to improve the invasion of osteoblast cells during osteointegration.

3.4. Mechanical properties

Fig. 7 shows the tensile fracture strength of pressed α-TCP pellets before hydrolysis together with those for CDHAp formed at 37 °C and 56 °C. The samples were hydrated for 36 h and 24 h, respectively. XRD analyzes revealed complete hydrolysis to HAp. The densities of the non-hydrated samples was around 56%, when consolidation pressure of 5.5 MPa was used. The average tensile strength of non-hydrated α-TCP was determined to be 0.70 MPa, with a standard deviation of 0.1 MPa. The fracture strengths of nine test samples varied from 0.58 to 0.82 MPa.

A significant increase in tensile strength was observed after hydrolysis. Strength values varied from 6.17 to 11.18 MPa and from 8.18 to 12.34 MPa for groups of 10 samples hydrated at 37 °C or 56 °C. The average values are 9.36 ± 0.4 MPa and 9.30 ± 0.5 MPa, respectively. The average densities were determined to be 70% after hydrolysis at 37 °C and 72% for hydrolysis at 56 °C. The density were obtained for triple measurements.

The small range of tensile strength values for the CDHAp formed is consistent with the degree of reaction accomplished at each temperature. Thus, the strength values determined for hydrated samples are representative for CDHAp, with the porosities and morphologies described. From a microstructural point of view the increase in fracture strength appears to be due to bridging of HAp needles forming reticulated structures between the solid grains as shown by the micrographs in Fig. 4.

For the non-stoichiometric apatite formed by hydrolysis of α-TCP compressive strength values of 15–16 MPa and tensile strength values of 2–3 MPa have been reported at a porosity of 60–70 vol % [10]. A wider range of compressive strength of 3–50 MPa has been reported by the same author within the porosity range of 55–80 vol % [17]. Improved mechanical properties have been reported for HAp formed by dissolution-precipitation reaction at 38 °C achieved by a uniform distribution of fine porosity [28]. In the present study, the tensile strength of CDHAp formed at physiological temperature has been determined as 9.36 ± 0.4 MPa for a porosity of 30 vol %. This value is in the range of reported tensile strengths by these literature citations.

4. Conclusions

The kinetics of calcium-deficient hydroxyapatite formation by direct hydrolysis of α-TCP were investigated. This cement-type reaction advances without formation of any other calcium phosphate phase other than phase-pure HAp. HAp formation is characterized by an initial period of wetting of the precursor powder, an induction period followed by growth during which bulk transformation to HAp occurs. Although the transformation mechanisms do not differ for particulate slurries and pre-formed pellets, the extent of HAp formation is limited in the compacted form. The microstructural appearance of HAp formed at 37, 45 and 56 °C is flake-like. The morphology of HAp formed at physiological temperature differs slightly from the HAp formed at higher temperatures. The HAp formed at 37 °C has smaller crystallite size compared to those formed at 45 °C and 56 °C. The extent of hydrolysis reaction in pre-formed pellets is controlled by the penetration of water to the reactant α-TCP sites. The hardening generated due to the hydrolysis was demonstrated by the increase in tensile strength of the pre-formed compacts of α-TCP. A 70% dense CDHAp formed from α-TCP at 37 °C can develop a tensile

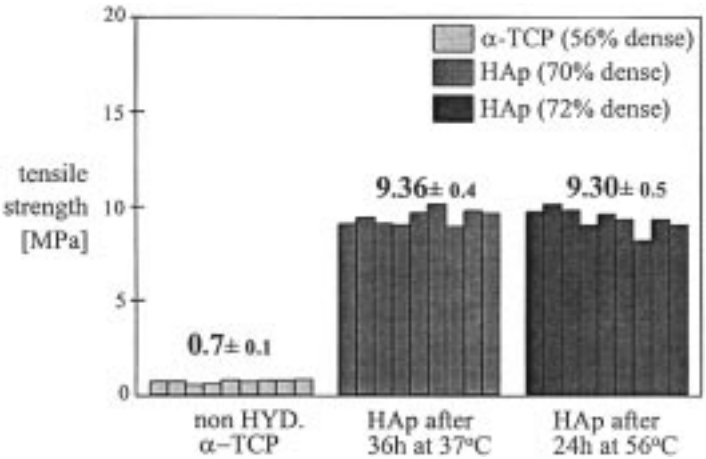

Figure 7 Fracture strength of pressed α-TCP and Ca-deficient HAp compacts formed by hydrolysis at 37 °C and 56 °C.

strength as high as 9.36 MPa from an original tensile strength of 0.70 MPa.

Acknowledgment

The authors gratefully acknowledge the support of National Science Foundation Grant DMR 951 0272.

References

1. W. VAN BRAEMDONCK, P. DUCHNEYNE and P. DEMEESTER, in ''Metal and ceramic biomaterials Vol II,'' edited by P. Ducheyne and G. W. Hastings (CRC Press, Boca Raton, FL, 1984) p. 144.
2. G. HEIMKE, *Angew. Chem* **101** (1989) 111.
3. M. E. EL DEEB, P. C. TOMPACH and A. T. MORSTAD, *J. Oral. Maxillofac. Surg.* **46** (1988) 955.
4. N. HASAKA and T. NAGATA, *ibid.* **45** (1987) 583.
5. J. F. KAY, M. JARCHO, G. LOGAN and S. T. LIU, *Trans. Soc. Biomat.* **9** (1986) 13.
6. S. HIGASHI, T. YAMAMURA, T. NAKAMURA, Y. IKADA, S. H. HYON and K. JAMSHIDI, *Biomaterials* **7** (1986) 183.
7. J. E. DEVIN, M. A. ATTAWIA and C. T. LAURENCIN, *J. Biomater. Sci. Polymer Edn* **7** (1996) 661.
8. M. KIKUCHI, Y. SUETSUSU, J. TANAKO and M. AKAO, *J. Mater. Sci.: Mater Med.* **8** (1996) 361.
9. W. E. BROWN and L. C. CHOW, in ''Cements Research Progress-1987'', edited by P. W. Brown (American Ceramic Society, Westerville, OH, 1988) p. 351.
10. H. MONMA and T. KANAZAWA, *Yogio-Kyoki Shi* **84** (1976) 209.
11. M. P. GINEBRA, M. G. BOLTONG, E. FERNANDEZ, J. A. PLANELL and F. C. M. DRIESSENS, *J. Mater. Sci.: Mater Med.* **6** (1995) 612.
12. K. S. TENHUISEN and P. W. BROWN, *Biomaterials* **20** (1999) 427.
13. P. LEAMY, P. W. BROWN, K. S. TENHUISEN and C. R. RANDALL, *J. Biomed. Mater. Res.* **42** (1998) 548.
14. R. I. MARTIN and P. W. BROWN, *ibid.* **35** (1997) 299.
15. E. J. PROSEN, P. W. BROWN, G. FROHNSDORFF and F. DAVIS, *Cem. Concr. Res.* **15** (1985) 703.
16. P. W. BROWN, R. I. MARTIN and K. S. TENHUISEN, in ''Bioceramics: Materials and Applications II'', edited by R. P. Rusin and G. S. Fischman (American Ceramic Society, Westerville, OH, 1996) p. 37.
17. H. MONMA, S. UENO and T. KANAZAWA, *J. Chem. Tech. Biotech.* **31** (1981) 15.
18. H. MONMA and M. NAGAI, in ''Inorganic Phosphate Materials'', edited by T. Kanazawa (Elsevier, Tokyo, Japan, 1988) p. 88.
19. S. GRAHAM and P. W. BROWN, *J. Crystal Growth* **5** (1995) 106.
20. K. S. TENHUSIEN, R. I. MARTIN, M. KLIMKIEWICZ and P. W. BROWN, *J. Biomed. Mater. Res.* **29** (1995) 803.
21. K. S. TENHUISEN and P. W. BROWN, *ibid.* **36** (1997) 306.
22. R. I. MARTIN, K. S. TENHUSIEN, P. LEAMY and P. W. BROWN, *J. Phys. Chem. B* **101** (1997) 9375.
23. B. O. FOWLER, E. C. MORENO and W. E. BROWN, *Arch. Oral Biol.* **11** (1966) 477.
24. R. Z. LEGEROS, G. DACULSI, I. ORLY, T. ABERGAS and W. TORRES, *Scan Microsc.* **3** (1989) 129.
25. R. Z. LEGEROS, in ''Calcium Phosphate in Oral Biology and Medicine'', edited by H. M. Meyers (Karger Publications, San Francisco, CA, 1991) p. 4.
26. J. C. HEUGHEBAERT and G. MONTEL, *Calcif. Tissue Int.* **34** (1982) 103.
27. J. J. KLAWITTER and S. F. HULBERT, *J. Biomed. Mat. Res. Symp.* **2** (1971) 161.
28. R. I. MARTIN and P. W. BROWN, *J. Mat. Sci.: Mater. Med.* **6** (1995) 138.

Received 29 September 1998
and accepted 29 April 1999